Flex-to-stretch hybrid electronics–bonding-free robust interface for wearable wireless physiological monitoring

Srinivas Gandla, Sunju Kang, Junho Kim, Yunjeong Yu, Jaeseong Kim, Hyeongtae Lim, Hyuk-Jun Kwon, Sung-Min Park, Sunkook Kim

***Abstract*—Hybrid electronics require a robust mechanical interface between externally fabricated stretchable sensors and flexible printed circuit boards (FPCBs) to obtain stable electrophysiological information. The most advanced technique for the integration of FPCBs with stretchable sensors is anisotropic conductive film bonding. Fabricating high-performance sensors requires microfabrication techniques, such as photolithography and etching, which are cumbersome and expensive. Therefore, a sensor fabrication process that supports FPCB manufacturing with lower complexity and cost is required. Herein, we propose a bonding-free approach for fabricating FPCBs and stretchable sensors on a single substrate. This approach utilizes in- and out-of-plane mechanical gradients to obtain a robust and durable mechanical interface for a smooth transition of the internal mechanical stress compliance, as confirmed by experiments and simulations. The gradient mesh patterns, without ACF bonding, can withstand tensile strains of over 30% before experiencing electrical breakdown. Additionally, Kirigami-inspired mesh patterns can extend stretchability by over 100%. The electrical performance of temperature sensors (linear response to temperature changes) and ECG sensors (clear visibility of PQRST peaks) remains stable under various physical activities. User-accessible, facile laser ablation and cutting techniques compatible with the FPCB manufacturing process were employed to fabricate stretchable sensors. This approach enables the development of FPCB-compatible on-skin stretchable sensors with robust mechanical properties.**

***Index Terms*—stretchable electronics, bonding-free, robust interface, physiological monitoring, laser ablation.**

I. INTRODUCTION

Wearable medical devices comprising flexible/stretchable sensors integrated with flexible printed circuit boards (FPCBs) that can serve and facilitate real-time point-of-care diagnosis are of significant interest owing to their ability to provide myriad services without human intervention.[1]–[4] With the rapid growth of the human population, the number of patients suffering from infections, diseases, or illnesses seeking care from hospitals is increasing. Therefore, it is difficult for hospital staff to manage and treat patients in crowded hospitals owing to tight schedules and limited space. Therefore, innovative, and inexpensive wearable devices that can ubiquitously and continually monitor primary vital signs, such as heart rate, blood pressure, and temperature, are required to transmit information via wireless communication in real-time to medical practitioners.[5] In addition, these devices can significantly reduce the physical involvement of doctors and patients in simple screening and hospital stays. This ubiquitous diagnostic capability has become important in the present COVID-19 scenario where patients have been less exposed to practitioners and other patients while receiving efficient consultation through telemedicine.[6] Monitoring the critical physiological parameters of the human body can also be important at industrial sites. The real-time monitoring of the physiological factors of workers at industrial sites, where there are several risks owing to physical work overload, can help prevent possible accidents.

This study was supported by the SKKU Research Fellowship Program of Sungkyunkwan University and the National Research Foundation of Korea 2021R1I1A1A01060078. This research was also supported by BrainLink program funded by the Ministry of Science and ICT through the National Research Foundation of Korea (RS-2023-00237308), the National Research Foundation of Korea (NRF-2022M3D1A2083618), National R&D Program through the National Research Foundation of Korea(NRF) funded by Ministry of Science and ICT(2021M3H4A1A03049084), and the Pioneer Research Center Program through the National Research Foundation of Korea funded by the Ministry of Science, ICT & Future Planning (2022M3C1A3081294). *(Srinivas Gandla, Sunju Kang, and Junho Kim contributed equally to this work.) (Corresponding author: Sunkook Kim; Sung-Min Kim; Hyuk-Jun Kwon).*

Srinivas Gandla, Sunju Kang, Yunjeong Yu, Jaeseong Kim, and Sunkook Kim are with the Department of Advanced Materials Science and Engineering, Sungkyunkwan University, Suwon 16419, South Korea. (e-mail: seonkuk@skku.edu)

Junho Kim and Sung-Min Park are with the Department of Convergence IT Engineering, Pohang University of Science and Technology, Pohang, South Korea. (e-mail: sungminpark@postech.ac.kr)

Hyeongtae Lim and Hyuk-Jun Kwon are with the Department of Electrical Engineering and Computer Science, Daegu Gyeongbuk Institute of Science and Technology (DGIST), Daegu, South Korea. (hj.kwon@dgist.ac.kr)

Sung-Min Park is with the School of Interdisciplinary Bioscience and Bioengineering, Pohang University of Science and Technology, Pohang, South Korea. (e-mail: sungminpark@postech.ac.kr)

The Institutional Review Board of an affiliated university approved the study (approval no. PIRB-2022-E020). In addition, all the participants were provided with information on the voluntary nature of the study, the freedom to withdraw their enrollment, and the strategies that would be adopted to protect their anonymity and confidentiality; subsequently, their written informed consent was obtained.

Wearable devices transitioning from rigid to flexible to stretchable have emerged to mitigate the interfacial mechanical mismatch between external sensor circuitry and soft skin.[7]–[9] FPCBs that are integrated with mechanically stretchable sensor circuitry processed by microfabrication techniques are referred to as Flexible-to-stretchable hybrid electronics (FSHE). While this approach offers an immediate solution, it is overall inefficient due to two main reasons. Firstly, the fabrication of stretchable sensors requires multiple patterning and etching procedures (including etching of polyimide substrates) that are tedious, labor-intensive, and expensive. Secondly, ACF bonding necessitates manual alignment, making the process inefficient.[2], [3] FSHE has the following features: i) hard components—an FPCB integrated with silicon-based IC components for computation, signal processing, and data transmission, ii) soft components—stretchable sensors for mimicking skin deformations and conformal interfaces, and iii) an interface between the hard (FPCB) electronics and soft sensors. The fabrication of serpentine-based stretchable sensors using conventional photolithography techniques would be challenging and laborious, especially when attempting to directly fabricate them on a single FPCB platform. Hence, a bonding-free single platform for the seamless integration of FPCBs and structural stretchable sensors stands as a technologically advanced and promising solution. This development is crucial for the creation of efficient and robust sensor acquisition devices, ensuring mechanical endurance. In addition, sensors fabricated on polyimide (PI) films are highly resilient to flexibility and possess a high yield strength under tensile stress.

Here, we demonstrate a bonding-free, single-platform, robust mechanical interface between structurally stretchable electrophysiological sensors (electrocardiography (ECG) and temperature) and an FPCB for wireless, real-time, and stable physiological monitoring. The bonding-free strategy utilizes an extended thin PI film, which is a middle layer for both the FPCB and sensors. A facile subtractive laser manufacturing technique was employed to fabricate the structurally stretchable sensors without any detrimental effects on the FPCB. The electrical and mechanical performances of the unbonded (bonding-free) test samples under externally applied mechanical tensile strains and cycles were better than those of the bonding sample, as confirmed via experimental and simulation results. The key contributions to be sought from this work are as follows: 1) the primary novelty is the bonding-free single platform approach for the manufacturing of FPCB and its associated structurally stretchable sensors: Bonding-free suggests a more streamlined and efficient manufacturing process, potentially reducing costs and complexity. The use of a single platform implies integration and consolidation of multiple steps or components, simplifying the overall production process; 2) a stretchable in-plane gradient serpentine widths pattern strategically designed to reduce interfacial stresses for improved durability and performance; 3) stable monitoring of electrophysiological signals during various physical activities: the stable monitoring serves as a crucial validation of the wearable device's performance robustness. Traditional metals, such as platinum and gold, are generally stable under moist conditions and are used as sensing materials. The temperature sensor exhibited a stable sensing performance under static and dynamic temperature loading conditions. During daily life activities, the wearable device delivered stable temperature, ECG, and acceleration signals with low noise.

II. Methods, Results, and discussion

A. Bonding-free single-substrate wearable device and sensor circuitry system

Figure 1A shows a schematic of the single-platform bonding-free wearable stretchable sensor system for the wireless monitoring of temperature and ECG on a personal mobile phone. The stretchable sensor circuitry is typically integrated with the FPCB using the ACF bonding technique.[1], [2], [14], [3], [4], [8]–[13] Moreover, structure-based stretchable sensors are predominantly fabricated using conventional microfabrication techniques, encompassing film deposition, spin-coating, photolithography, developing, and etching procedures. This process involves the dry etching of the underlying supporting film, typically PI, through oxygen plasma to create stretchable filamentary circuitry.[11], [15], [16] In addition to stretchable sensors/devices, stretchable Flexible Printed Circuit Boards (FPCBs) have also been developed to create complete stretchable hybrid devices.[17]–[19] However, these fabrication processes are cumbersome and expensive. By contrast, additive and subtractive manufacturing techniques have attracted considerable interest owing to their ease of fabrication, programmability, low cost, and rapid processing. Unlike additive manufacturing, such as 3D printing, where the material is deposited layer-by-layer to construct an object, subtractive manufacturing involves the removal of excess parts after cutting the film (supporting) into desired structure-based patterns using a mechanical blade or photo/thermal laser cutter. In the case of blade-cutting techniques, functional material patterning, similar to the patterning of Au on a film, is not possible.[20]–[23] By contrast, both functional material patterning and film cutting are possible in the case of laser processing technology.[12], [13], [24] A laser ablation technique with optimal laser parameters can be used to pattern functional materials using a hatch tool without damaging the underlying supporting film, whereas the laser cutting process is executed along the layout of the design pattern. Moreover, selective laser sintering[25]–[27] and laser-induced carbonization/graphitization[10], [28], [29] are two other promising approaches currently being extensively researched for patterning nano/micro functional materials. However, stretchable films prepared using these techniques exhibit notable changes in resistance when subjected to external mechanical strain stimuli, primarily due to their slightly increased film thickness at the micro-scale.

The system requires not only a bonding-free platform but also robust mechanical endurance. Regardless of the bonding technique used, a significant difference in material moduli on either side of the interface can lead to sharp changes in stresses when subjected to external loads. Thus, it is crucial to carefully design the interface for robust mechanical tolerance. Gradient structures observed in nature, such as bone-cartilage gradient interface tissue, provide mechanical resilience.[30] Inspired by nature, researchers have used gradient modulus structures to ensure a highly resilient stretchable system. [31]–[36] To date, two in- and out-of-plane gradient structures have been reported. A finite element method (FEM) simulation was used to analyze the gradient modulus structures to explore the stress-energy absorption mechanism. Therefore, bonding-free, and mechanical gradient thicknesses and patterns were adopted in this study.

A flexible-to-stretchable sensor system designed on a single substrate with an in-plane structurally stretchable serpentine width gradient pattern comprising temperature and ECG sensors and an out-of-plane thickness gradient from the center of the FPCB (~86 µm) to outward sensors (~12 µm) is shown in Figure 1b. The characteristics of the in-plane and out-of-plane are the serpentine width gradient pattern and gradient thickness: these features ensure a smooth transition of internal mechanical stress compliance, thereby establishing a robust and durable mechanical interface. The gradient thickness from the FPCB to the sensor is shown in Figure 1c. Real and simulated images of serpentine mesh patterns of uniform and in-plane gradient serpentine widths at 30% strain, where a large stress concentration developed at the flexible stretchable interface, are presented in Figures 1d and 1e. Further details are discussed in the following section.

The fabrication process of the single-substrate bonding-free wearable device is shown in Figure 2a. The overall fabrication process involves two techniques: i) routine conventional microfabrication-based techniques for the manufacture of FPCB (see Supplementary Material), and ii) unconventional subtractive laser processing techniques for preparing stretchable sensors (see Video SV1). Initially, multilayers, such as top PI, top Cu, middle PI with via, and bottom Cu, were heat pressed for lamination, and then IC chips were soldered onto the FPCB. The middle PI film was used as a supporting film for sensor fabrication. The FPCB with bonded rigid components and an extended large area of thin PI film is shown in Figure S1. The concept of extended electrodes can be applied to the work that has been recently reported.[37] The laminated stack was then placed on an acrylic substrate with a thermal release tape between them. The metals (platinum for temperature and gold for ECG electrodes) were deposited successively via e-beam on the other side of the middle PI film using shadow masks. The shadow masks were prepared using a UV laser cutting machine (Inno6, Korea) with processing parameters; focal distance (225 mm), power (6 W), speed (2000 mm/s), and current (5 A). Subsequently, an infrared laser (INLASER Co., Ltd.) with a wavelength of 1064 nm was used for patterning the Pt and Au metals for temperature and ECG sensors, respectively using a laser ablation technique. The IR laser processing parameters are the focal distance (210.5 mm), power (40%), frequency (20 kHz), speed (1000 mm/s), and pulse width (4 ns). Followed by the deposition of Al_2O_3 via atomic layer deposition as a passivation layer. For passivation, two other alternatives such as Parylene-c and PTFE which are industrially viable can also be used due to their electrical insulation, moisture barrier, and chemical-resistant properties. The alternative passivation layers UV laser cutting was performed using alignment markers to enable the stretchability of the patterned metal films. Finally, the sensor device was peeled off from the thermal release tape after being placed on a hotplate at 100 °C. An expanded view of the sensor device is shown in Figure 2b. Also, see the sensors fabricated away from the FPCB part (Figure S2). A real image of the FPCB with components (labeled) facing the top and an illustration of the ECG and temperature sensors are shown in Figure 2c. The real image of the sensor device with a T&L patch is shown in Figure S3. The detailed layout of the FPCB is shown in Supplementary Figure S4. Furthermore, the components information and design of FPCB are shown in Figure S5 and Table S1.

The circuit for recording temperature and ECG consists of a microcontroller unit (MCU) with BLE communication, a constant current source (CCS), an analog-to-digital converter (ADC) to measure the resistance of the temperature sensor, an analog front-end (AFE) for ECG, and power management (PM). An MCU supporting BLE, CC2640R2F (Texas Instruments, USA), was used for data acquisition and wireless communication with a smartphone. The CCS was implemented using a Howland current pump to measure the resistance of the temperature sensors. When the resistance of the sensor changes according to the temperature, the CCS changes the voltage applied to the sensor such that a constant current flows. The change in the resistance of the sensor can be measured by measuring this voltage, which indicates that the temperature can be measured (Figure 2d). The voltage applied to the sensor is digitalized by an ADC IC, MCP3561 (Microchip Technology, USA), and the MCU communicates with MCP3561 to acquire data. The voltage difference between the two ECG electrodes was amplified, filtered, and digitalized using an AFE IC MAX30003 (Maxim Integrated, USA) (Figure 2e). An accelerometer (ACC), MC3672 (mCube, USA), was used to measure the acceleration along three axes to record the user activity. The MCU collects the ECG, temperature, and three-axis acceleration data and sends them to the smartphone via BLE5. The board is made of an FPCB for use in patch form. Every second, the AFE device transmits a total of 184 bytes of data via BLE, which includes 128 bytes from ECG measurements, 42 bytes of 10-bit data from the accelerometer's X, Y, and Z axes, and 14 bytes of 24-bit voltage data from the temperature sensor.

B. Experimental and computational studies of flex-to-stretch serpentine mesh patterns

Experimental measurements and FEM simulations demonstrate the essential mechanics, as summarized in Figure 3. Experimental measurements were conducted by simultaneously measuring the mechanical load and electrical resistance under externally applied tensile strains. Mechanical

This article has been accepted for publication in IEEE Internet of Things Journal. This is the author's version which has not been fully edited and content may change prior to final publication. Citation information: DOI 10.1109/JIOT.2024.3350022

measurements of the test samples were conducted using an ultimate tensile machine from Mark 10 Corp. (model ESM303). The optical images of the test samples (mesh patterns of the metal layers) captured at $\geq 30\%$ applied tensile strains with (with and without gradient width patterns) and without (with gradient width patterns) ACF bonding are shown in the first column of Figures 3a-c. For greater reliability of the FEM analysis, the results obtained from the simultaneous measurement of load/strain and electrical/strain responses were compared with the FEM simulation results. The Young's modulus value of the PI used in the simulation was calculated from the linear slope of the stress-strain curve (Figure S6). The test samples used in the simulations and experiments consisted of a free-standing multilayer stack pattern (PI (12 μm)/Ti (5 nm)/Au (100 nm)/Al_2O_3 (50 nm)) similar to that used in the sensor fabrication. The criteria for the gradient part are summarized in the Supplementary Materials (figures S7 and S8). The test samples were designed to have the same bonding areas, sizes, and thicknesses. Initially, the effect of only the gradient case on the ACF-bonded samples was examined. Subsequently, the gradient case without ACF bonding (single-substrate bonding-free) was also examined to compare the samples with and without ACF bonding. Both cases with and without a gradient in the ACF-bonded samples showed identical resistance and load variations over the entire range of tensile strains, from 0 % to 40 %; however, the principal strain in the metal layers developed near the bonding interface was relatively higher in the case without a gradient, which was also confirmed by the FEM results (Figure 3a, b). Thus, stretchability is limited by the mesh pattern itself, in the case without a gradient, because of the induced intrinsic stress generated within the metal layers. With increasing applied strain (from 0% to 10%–15%), the serpentine arcs tend to stretch with in- and out-of-plane bending by minimizing the principal strain in the metal layers. With a further increase in the strain, the samples experienced a steady increase in load until the breakdown. In this region, the load/strain response is linear, where the samples can endure a fatigue test and rupture of the material under repeated strain cycles. During the linear increase in load up to ~30% applied strain, the serpentine arcs experience stresses that cause an increase in the principal strain in the metal layers, inducing deformation in the thin Au film, resulting in an increase in resistance with strain. According to the literature, the stretchability range of human skin lies within 30% strain [9]; therefore, the sensor structure withstanding 30% uniaxial strains is a criterion for the sensors to function smoothly when worn on the skin during physical movements. Once the applied strain surpasses the structural limit of the sample, the mesh pattern causes the resistance to change abruptly. Moreover, the breakdown of samples occurs mostly at the interface owing to sharp load enduring variations in the materials on either side of the interface; one side of the interface is a pattern-free PI film that endures high loading, and the other side is a mesh pattern that endures low loading. Although the load/strain responses with and without a gradient appear identical, the simultaneous resistance/strain responses exhibit magnitude variations, which reveals the importance of the gradient width pattern. The relative change in resistances in the case without a gradient at 30% applied strain is approximately four times higher than that with a gradient. This is because of the relatively higher principal strains developed in the metal layers near the interface in the case without a gradient. It is apparent from both the experimental and simulation analyses that the gradient pattern ensures a smooth transition of the principal strain in the metal layers along the tensile strain direction. This highlights the utility of gradient patterns. Despite the better results of the ACF-bonded samples with a gradient, the ACF-bonded samples can deteriorate in fatigue tests under repeated mechanical loading. Before that, the ACF-bonding-free sample was examined, as described above. This approach can prevent any mechanical failure arising from the relatively weak bonding in ACF-bonded samples. Comparatively, bonding-free samples with a gradient pattern exhibited better results. As mentioned earlier, to gain more insight into the mechanical durability of ACF-bonded samples with and without a gradient, fatigue tests were performed by applying cyclic strain between 0% and 20%. For the ACF-bonded sample, the relative change in resistance increased significantly by 11% after 200 cycles and continued to increase at a rate of 34% up to 5000 cycles (Figure S9). By contrast, the bonding-free sample initially showed a lower relative change in resistance, which continued to increase by ~2% from 2000 to 5000 cycles. Although the gradient pattern in the cases with and without ACF bonding showed similar results, the bonding-free sample demonstrated better durability, which is an essential requirement for practical viability. Currently, the reason for the deterioration of the ACF-bonding samples under repeated mechanical loading is unclear, but it may be due to the propagation of small cracks at the metal-to-metal bonding interface. Notably, the serpentine-based mesh pattern can be further modified to increase operational stretchability, as shown in Figure S10.

The FEA simulation results for with and without out-of-plane gradient thickness are shown in Figure S11a and b. In both cases, the maximum stress generated at the thickness variation interface is visible; in the case without gradient, the internal stress is higher and distributed starting from the interface to the thin film while in the case with gradient, the stress is concentrated at the interface without much stress generation within the thin film. This is also true in the case of in-plane serpentine patterns without gradient structure, in which the stress generation is higher extending from the interface to the thin-film serpentine pattern side (Figure 1d, simulation part). Thus, the out-of-plane structure with gradient thickness can endure stresses with less effect on the relatively thin film. In summary, the bonding-free gradient pattern sample demonstrated better endurance and durability.

C. Characteristics of temperature, ECG, and acceleration sensors

Wearable sensors for the real-time continuous monitoring of electrophysiological signals, such as temperature and ECG, from the peripheral body are of significant interest, as they can provide contextual information that would aid on-site medical diagnosis. For the reliable monitoring of human body temperature, the sensitivity of temperature sensors is important to detect small temperature changes (<0.5 °C). Usually, the human body temperature is between 30 and 40 °C. The noble metal platinum is a preferred choice as a temperature-sensing material due to its stable, hysteresis-free, and linear electrical responses to changes in human body temperatures.[2], [38]–[40] Additionally, advanced nanomaterials and 2D materials have garnered attention as potential sensing materials because of their noteworthy electrical properties, as previously discussed in various reports.[41], [42] However, the feasibility of these materials as suitable candidates for sensors requires further investigation. Furthermore, unique metals and semiconductors have demonstrated promising results in this field, positioning them as potential candidates for future sensor applications.[43], [44]

The temperature sensor characteristics are evaluated by placing the sensor on a variable heat source assembled at the I–V probe station (Keithley 4200-SCS). The electrical responses (relative change in resistance $\Delta R/R_0$) to temperature are shown in Figure 4. The sensor response to a systematic increase in the temperature is shown in Figure 4a. The sensitivity of the temperature sensor is defined as the temperature coefficient of resistance (TCR). The TCR is expressed as the relative change in resistance to the temperature changed by 1 ºC that is $\Delta R/(R_0\times\Delta T) = R\text{-}R_0/(R_0\times T\text{-}T_0)$, where ΔR denotes the change in resistance corresponding to the change in temperature ΔT and R and R_0 are resistance and initial resistance at temperature T and T_0. From Figure 4a and the above formula, the TCR value of the temperature sensor is about 0.11%/ºC. The resistance of the sensor at 30 °C (Rt@30) depends on its geometry and dimensions. The serpentine geometry with an 80-µm metal (Pt) width over a length of 1 cm resulted in an Rt@30 of 500 kΩ. The temperature varied in intervals of 0.2 °C. The resistance versus temperature graph shows that, with a continuous rise in temperature in intervals of 0.2 °C, an apparent linear increase in resistance can be observed. The linearity index R^2 extracted from the linear fit to the experimental data is approximately 0.9997, which indicates that the sensor response is linear to temperature changes. This is essential because nonlinear responses require additional programming to assign calibrated resistance variations to temperatures. Subsequently, a static temperature stability test was performed by subjecting the sensor to a longer duration of constant temperature in steps of 1 °C. The sensor exhibited a stable response to the temperature (Figure 4b). The sensor response to cyclic changes in temperature at intervals of 0.2 °C was mostly stable with a distinguishable separation among the relative data points (Figure 4c). A dynamic temperature test was performed using continuous cyclic variations of temperatures ranging from 22 °C to 32 °C. The results showed a steady response to the temperature changes. Note that the rise and fall responses to temperature were limited by the measuring instrument. Finally, the data collected for the continuous real-time monitoring of body temperatures for ~40 minutes for the wearable device worn on the lower left rib cage of a healthy male volunteer are graphically shown in Figure 4e. The temperature data were recorded at a sampling rate of 1 Hz and a resolution of 24 bits. During monitoring, the subjects were asked to follow their usual activities. Temperature sensors with high linearity (R_2 = 0.9997), a low minimum limit of detection (0.2 °C), and stability attributes are promising for reliable temperature sensor applications.

Another important electrophysiological signal is ECG, which is used to diagnose the health status of patients in cardiology. The ECGs provide essential information about heart function, aiding in the detection of irregular rhythms like atrial fibrillation, early signs of conditions such as myocardial ischemia and heart attacks, and the evaluation of cardiac and psychophysiological fitness through stress tests.[45] ECGs also diagnose symptoms and identify heart issues proactively. ECGs play a pivotal role in assessing patients before heart surgeries, serving as the cornerstone of heart health assessment, diagnosis, and care, guiding healthcare decisions for improved cardiac well-being.

Changes in the PQRST peaks of an ECG can be critical indicators of cardiac health. Alterations in these peaks, such as irregular P-waves, QRS complex changes, or ST-segment deviations, may signal conditions like arrhythmias, ischemia, or myocardial injury, with potentially serious health consequences if left unaddressed.[46] Timely recognition and intervention are essential for preserving overall well-being.

Unlike clinical settings where 10-electrode measurements are used, wearable devices use a bipolar electrode setup (Figure 5a, b). Although a three-electrode wearable device cannot provide a complete picture of heart activity, it provides a necessary picture of heart electrical activity; moreover, because of its compactness and portability, it increases patient comfort. In the three-electrode configuration, two electrodes (bipolar) are used to measure the surface potential difference, and the third electrode (ground) is used for noise reduction. The measured raw ECG signal from the wearable device is shown in Figure 5c, while Figure 5d shows the magnified view of the signal with a highlighted green section. The ECG signal was recorded while sitting in a resting position. During physical movement, the device remained intact on the skin because of the stickiness and stretchability of the patch. Bipolar stretchable electrodes aligned with the center of the FPCB were placed on the left side of the chest, mimicking the precordial lead V2. At this position, the device can capture all the details of the human ECG, including the P wave, QRS complex, T wave, ST-segment, and J-point; all the peaks are labeled in Figure 5d. The device can deliver high-temporal-resolution data with low-noise signals and a pk-pk magnitude of ~0.4 mV. The Pan–Tompkins algorithm was used to obtain the R peak, which is one of the characteristic points of the ECG[47]. A flowchart representing the signal processing for detecting the R peak of the ECG is shown in Figure 5e. The ECG raw data were band-pass filtered to remove baseline wander and high-frequency noise, and cutoff frequencies of 3 and 40 Hz were used. The filtered data were differentiated to obtain information on the slope of the QRS. It was squared to remove the error caused by the T wave, and the duration information of the QRS was obtained by moving-window integration. The noise level, signal level, and threshold were adjusted to reduce errors, and finally, the R-peak was determined. In addition, sample entropy (SampEn), a method used to evaluate the complexity of time-series signals, was used to analyze the heart rate of the measured ECG signal. The sampling rate and resolution of the ECG data were 128 Hz and 8 bits, respectively. A comparison of our wearable device sensors and features with previous studies is presented in Table S2.[1], [2], [52], [3], [10], [37], [44], [48]–[51]

D. Electrophysiological monitoring during various activities

The validation of the wearable device's performance was evaluated under various physical activities by human volunteers, such as cycling, walking up and down stairs, and before and after drinking alcohol (Figure 6). For this study, a wearable device with a T&L patch attached to the chest was used (also see a wearable device attached with Tegaderm and medical bandage onto the skin, Figure S12). The patch from T&L Co., Ltd. consists of the following two layers: (1) a protection layer made of polyurethane film, which can protect the human skin and sensor modules from the outer environment; and (2) an absorbing and adhesive layer made of silicone and polyurethane film—with double-sided adhesion to adhere it to the integrated sensor and FPCB module—which protects the skin from allergies and provides conformability while attaching the sensor device to the human body. The other types of patches used in the study are 3M Tegaderm and medical textile bandages (NASARA, Kinesiology tape).

The physical activity study also used an acceleration sensor integrated into the FPCB. The X, Y, and Z acceleration data were measured with a sampling rate of 14 Hz and a resolution of 10 bits. All the data were collected by the MCU for 1 s and sent to the smartphone application via BLE. All recorded ECG signals in Figure 6 are presented by selecting an 8-second segment from the entire measured dataset to facilitate the easy visualization of waveform variations. The variation in the R-R interval time series is considered sample entropy (SampEn). During indoor cycling, the ECG signals recorded before (10 min) and after (10 min) cycling showed a different heart rate, represented as R-R intervals (Figure 6a). The SampEn values obtained from three different volunteers, cases 1, 2, and 3, are shown in the same figure. Similarly, the ECG signals showed an increase and decrease in heart rate while the volunteers walked up and down the stairs (Figure 6b). Simultaneously, the X, Y, and Z acceleration data of the gyro for the volunteers walking up and down the stairs were distinguishable. The last activity, alcohol consumption, was evaluated by examining the ECG signals before and during alcohol consumption (first 15 min followed by second 15 min). According to a World Health Organization report, severe chronic alcohol intake can result in alcoholic cardiomyopathy and cause approximately 2.5 million deaths annually. Therefore, the real-time monitoring of ECG signals during alcohol consumption is essential to avoid excessive alcohol intake. Although this study does not consider an alarm alerting user on a mobile phone, it can provide sufficient information to practitioners when used in clinical and hospital environments. The ECG signals recorded before and during a 30-minute of alcohol consumption (300 mL, 13%) are shown in Figure 6c. During the first 15 minutes of consumption (150 mL), the heart rate decreased relatively compared with that before consumption and even decreased further with an additional 150 mL of consumption. The SampEn values obtained from three different volunteers (cases 1, 2, and 3) also showed a decreasing trend (Figure 6c). Note that, during all the activities, the temperature remained unchanged; therefore, the data were not included. A video of a volunteer walking on stairs up and down for real-time continuous monitoring of temperature, ECG, and acceleration (X, Y, and Z axes) is shown in Video SV2. The sensor system delivering stable ECG signals while performing physical self-body movements is shown in Video SV3. The stable operation of wearable devices is technically important for a robust environment. Based on the results of real-time monitoring of daily life activities, the wearable device successfully delivered the required electrophysiological signals without any failure. Therefore, the ability to maintain stable monitoring of electrophysiological signals enhances the practical usability and real-world applicability of the wearable device, making it suitable for a broader range of users and applications.

III. Conclusion

A bonding-free, single-platform, hybrid sensor acquisition device system for the wireless monitoring of temperature and ECG on a personalized mobile phone was successfully demonstrated. Subtractive laser ablation and cutting techniques performed using an infrared nanosecond laser, which is facile and safe, were utilized to fabricate stretchable sensors adjacent to the FPCB directly. The flexible-to-stretchable system utilizes in- and out-of-plane gradient structures for a robust mechanical platform, confirmed by the experimental and simulation results. The temperature sensor performances are stable and exhibit linear characteristics, however, advanced functional materials can be employed to further enhance sensitivity. It is important to note that the deposition of these functional materials should be compatible with the overall fabrication process. The current manufacturing approach can be extended to fabricate sensors covering areas as large as 15 cm, allowing for full-scale body monitoring. The ACF bonding, involving human intervention, of stretchable sensors with many circuitries to the FPCB would be critical, while the current approach resolves this issue effortlessly. Despite the many advantages of laser fabrication, one of the key limiting factors is the limited resolution, typically in the range of 20-50 µm. Achieving resolutions below this range could be possible to some extent but may come at the expense of increased time. Through the current approach, wearable sensor technology benefits considerably from the rapid processing of sensors, low-cost manufacturing, and robustness of the device. Overall, the wearable device presented herein offers unprecedented ease in collecting the electrophysiological data required to evaluate immunological irregularities during daily life activities.

References

[1] Y. Khan *et al.*, "Flexible Hybrid Electronics: Direct Interfacing of Soft and Hard Electronics for Wearable Health Monitoring," *Adv. Funct. Mater.*, vol. 26, no. 47, pp. 8764–8775, Dec. 2016, doi:

10.1002/adfm.201603763.

[2] S. Lee *et al.*, "All-Day Mobile Healthcare Monitoring System Based on Heterogeneous Stretchable Sensors for Medical Emergency," *IEEE Trans. Ind. Electron.*, vol. 67, no. 10, pp. 8808–8816, Oct. 2020, doi: 10.1109/TIE.2019.2950842.

[3] Y. Kim *et al.*, "All-in-One, Wireless, Stretchable Hybrid Electronics for Smart, Connected, and Ambulatory Physiological Monitoring," *Adv. Sci.*, vol. 6, no. 17, p. 1900939, Sep. 2019, doi: 10.1002/advs.201900939.

[4] J. Oh *et al.*, "Air-Permeable Waterproofing Electrocardiogram Patch to Monitor Full-Day Activities for Multiple Days," *Adv. Healthc. Mater.*, vol. 11, no. 12, p. 2102703, Jun. 2022, doi: 10.1002/adhm.202102703.

[5] M. Hasan, M. Shahjalal, M. Chowdhury, and Y. Jang, "Real-Time Healthcare Data Transmission for Remote Patient Monitoring in Patch-Based Hybrid OCC/BLE Networks," *Sensors*, vol. 19, no. 5, p. 1208, Mar. 2019, doi: 10.3390/s19051208.

[6] A. Channa, N. Popescu, J. Skibinska, and R. Burget, "The Rise of Wearable Devices during the COVID-19 Pandemic: A Systematic Review," *Sensors*, vol. 21, no. 17, p. 5787, Aug. 2021, doi: 10.3390/s21175787.

[7] D.-H. Kim *et al.*, "Epidermal Electronics," *Science (80-.).*, vol. 333, no. 6044, pp. 838–843, Aug. 2011, doi: 10.1126/science.1206157.

[8] K.-I. Jang *et al.*, "Rugged and breathable forms of stretchable electronics with adherent composite substrates for transcutaneous monitoring," *Nat. Commun.*, vol. 5, no. 1, p. 4779, Dec. 2014, doi: 10.1038/ncomms5779.

[9] L. Tian *et al.*, "Large-area MRI-compatible epidermal electronic interfaces for prosthetic control and cognitive monitoring," *Nat. Biomed. Eng.*, vol. 3, no. 3, pp. 194–205, Mar. 2019, doi: 10.1038/s41551-019-0347-x.

[10] S. Gandla *et al.*, "Highly Linear and Stable Flexible Temperature Sensors Based on Laser-Induced Carbonization of Polyimide Substrates for Personal Mobile Monitoring," *Adv. Mater. Technol.*, vol. 5, no. 7, p. 2000014, Jul. 2020, doi: 10.1002/admt.202000014.

[11] N. Kim, T. Lim, K. Song, S. Yang, and J. Lee, "Stretchable Multichannel Electromyography Sensor Array Covering Large Area for Controlling Home Electronics with Distinguishable Signals from Multiple Muscles," *ACS Appl. Mater. Interfaces*, vol. 8, no. 32, pp. 21070–21076, Aug. 2016, doi: 10.1021/acsami.6b05025.

[12] H. Chae *et al.*, "Laser-Processed Nature-Inspired Deformable Structures for Breathable and Reusable Electrophysiological Sensors toward Controllable Home Electronic Appliances and Psychophysiological Stress Monitoring," *ACS Appl. Mater. Interfaces*, vol. 11, no. 31, pp. 28387–28396, Aug. 2019, doi: 10.1021/acsami.9b06363.

[13] S. Gandla *et al.*, "Ultrafast Prototyping of Large-Area Stretchable Electronic Systems by Laser Ablation Technique for Controllable Robotic Arm Operations," *IEEE Trans. Ind. Electron.*, vol. 69, no. 4, pp. 4245–4253, Apr. 2022, doi: 10.1109/TIE.2021.3073355.

[14] Y. Jiang *et al.*, "Topological supramolecular network enabled high-conductivity, stretchable organic bioelectronics," *Science (80-.).*, vol. 375, no. 6587, pp. 1411–1417, Mar. 2022, doi: 10.1126/science.abj7564.

[15] W.-H. Yeo *et al.*, "Multifunctional Epidermal Electronics Printed Directly Onto the Skin," *Adv. Mater.*, vol. 25, no. 20, pp. 2773–2778, May 2013, doi: 10.1002/adma.201204426.

[16] S. Xu *et al.*, "Stretchable batteries with self-similar serpentine interconnects and integrated wireless recharging systems," *Nat. Commun.*, vol. 4, no. 1, p. 1543, Feb. 2013, doi: 10.1038/ncomms2553.

[17] H. Kim *et al.*, "Fully Integrated, Stretchable, Wireless Skin-Conformal Bioelectronics for Continuous Stress Monitoring in Daily Life," *Adv. Sci.*, vol. 7, no. 15, p. 2000810, Aug. 2020, doi: 10.1002/advs.202000810.

[18] S. Xu *et al.*, "Soft Microfluidic Assemblies of Sensors, Circuits, and Radios for the Skin," *Science (80-.).*, vol. 344, no. 6179, pp. 70–74, Apr. 2014, doi: 10.1126/science.1250169.

[19] K.-I. Jang *et al.*, "Self-assembled three dimensional network designs for soft electronics," *Nat. Commun.*, vol. 8, no. 1, p. 15894, Jun. 2017, doi: 10.1038/ncomms15894.

[20] Z. Yan *et al.*, "Highly stretchable and shape-controllable three-dimensional antenna fabricated by 'Cut-Transfer-Release' method," *Sci. Rep.*, vol. 7, no. 1, p. 42227, Sep. 2017, doi: 10.1038/srep42227.

[21] S. Yang, E. Ng, and N. Lu, "Indium Tin Oxide (ITO) serpentine ribbons on soft substrates stretched beyond 100%," *Extrem. Mech. Lett.*, vol. 2, pp. 37–45, Mar. 2015, doi: 10.1016/j.eml.2015.01.010.

[22] S. Yang *et al.*, "'Cut-and-Paste' Manufacture of Multiparametric Epidermal Sensor Systems," *Adv. Mater.*, vol. 27, no. 41, pp. 6423–6430, Nov. 2015, doi: 10.1002/adma.201502386.

[23] M. Zhuang *et al.*, "Highly Robust and Wearable 37 Expression Recognition via Deep-Learning-Assisted, Soft Epidermal Electronics," *Research*, vol. 2021, Jan. 2021, doi: 10.34133/2021/9759601.

[24] Q. Yang *et al.*, "High-speed, scanned laser structuring of multi-layered eco/bioresorbable materials for advanced electronic systems," *Nat. Commun.*, vol. 13, no. 1, p. 6518, Oct. 2022, doi: 10.1038/s41467-022-34173-0.

[25] H. Jin Nam, J. Hun Yuk, Y.-S. Eom, J. Joo, K.-S. Choi, and S.-H. Choa, "Large-Scale Rapid Laser Sintering of Highly Stretchable Electrodes Using a Homogenized Rectangular Laser Beam," *J. Nanosci. Nanotechnol.*, vol. 21, no. 5, pp. 2959–2968, May 2021, doi: 10.1166/jnn.2021.19135.

[26] S. Liu, M. C. Yuen, and R. Kramer-Bottiglio, "Reconfigurable electronic devices enabled by laser-sintered liquid metal nanoparticles," *Flex. Print. Electron.*, vol. 4, no. 1, p. 015004, Feb. 2019, doi: 10.1088/2058-8585/aafa3b.

[27] S. Liu *et al.*, "Laser Sintering of Liquid Metal Nanoparticles for Scalable Manufacturing of Soft and Flexible Electronics," *ACS Appl. Mater. Interfaces*, vol. 10, no. 33, pp. 28232–28241, Aug. 2018, doi: 10.1021/acsami.8b08722.

[28] M. G. Stanford *et al.*, "High-Resolution Laser-Induced Graphene. Flexible Electronics beyond the Visible Limit," *ACS Appl. Mater. Interfaces*, vol. 12, no. 9, pp. 10902–10907, Mar. 2020, doi: 10.1021/acsami.0c01377.

[29] J. Edberg, R. Brooke, O. Hosseinaei, A. Fall, K. Wijeratne, and M. Sandberg, "Laser-induced graphitization of a forest-based ink for use in flexible and printed electronics," *npj Flex. Electron.*, vol. 4, no. 1, p. 17, Aug. 2020, doi: 10.1038/s41528-020-0080-2.

[30] Z. Liu, M. A. Meyers, Z. Zhang, and R. O. Ritchie, "Functional gradients and heterogeneities in biological materials: Design principles, functions, and bioinspired applications," *Prog. Mater. Sci.*, vol. 88, pp. 467–498, Jul. 2017, doi: 10.1016/j.pmatsci.2017.04.013.

[31] R. Libanori *et al.*, "Stretchable heterogeneous composites with extreme mechanical gradients," *Nat. Commun.*, vol. 3, no. 1, p. 1265, Jan. 2012, doi: 10.1038/ncomms2281.

[32] Z. Wei and X. Xu, "Gradient design of bio-inspired nacre-like composites for improved impact resistance," *Compos. Part B Eng.*, vol. 215, p. 108830, Jun. 2021, doi: 10.1016/j.compositesb.2021.108830.

[33] N. Naserifar, P. R. LeDuc, and G. K. Fedder, "Material Gradients in Stretchable Substrates toward Integrated Electronic Functionality," *Adv. Mater.*, vol. 28, no. 18, pp. 3584–3591, May 2016, doi: 10.1002/adma.201505818.

[34] Z. Wu *et al.*, "Seamless modulus gradient structures for highly resilient, stretchable system integration," *Mater. Today Phys.*, vol. 4, pp. 28–35, Mar. 2018, doi: 10.1016/j.mtphys.2018.02.002.

[35] N. Matsuhisa *et al.*, "Printable elastic conductors with a high conductivity for electronic textile applications," *Nat. Commun.*, vol. 6, no. 1, p. 7461, Jun. 2015, doi: 10.1038/ncomms8461.

[36] R. Moser *et al.*, "From Playroom to Lab: Tough Stretchable Electronics Analyzed with a Tabletop Tensile Tester Made from Toy-Bricks," *Adv. Sci.*, vol. 3, no. 4, p. 1500396, Apr. 2016, doi: 10.1002/advs.201500396.

[37] L. Yin *et al.*, "Chest-scale self-compensated epidermal electronics for standard 6-precordial-lead ECG," *npj Flex. Electron.*, vol. 6, no. 1, p. 29, May 2022, doi: 10.1038/s41528-022-00159-7.

[38] M. Naqi *et al.*, "A Fully Integrated Flexible Heterogeneous Temperature and Humidity Sensor-Based Occupancy Detection Device for Smart Office Applications," *Adv. Mater. Technol.*, vol. 4, no. 12, p. 1900619, Dec. 2019, doi: 10.1002/admt.201900619.

[39] M. Schepperle, M. Ghanam, A. Bucherer, T. Gerach, and P. Woias, "Noninvasive platinum thin-film microheater/temperature sensor array for predicting and controlling flow boiling in microchannels," *Sensors Actuators A Phys.*, vol. 345, p. 113811, Oct. 2022, doi: 10.1016/j.sna.2022.113811.

[40] R. W. Bertram, "TESTING AND STANDARDS FOR THERMAL

SOLAR COLLECTORS," in *Solar Energy Conversion II*, Elsevier, 1981, pp. 73–91.

[41] M. M. Hasan and M. M. Hossain, "Nanomaterials-patterned flexible electrodes for wearable health monitoring: a review," *J. Mater. Sci.*, vol. 56, no. 27, pp. 14900–14942, Sep. 2021, doi: 10.1007/s10853-021-06248-8.

[42] D. Jariwala, V. K. Sangwan, L. J. Lauhon, T. J. Marks, and M. C. Hersam, "Emerging Device Applications for Semiconducting Two-Dimensional Transition Metal Dichalcogenides," *ACS Nano*, vol. 8, no. 2, pp. 1102–1120, Feb. 2014, doi: 10.1021/nn500064s.

[43] M. Jung *et al.*, "Amorphous FeZr metal for multi-functional sensor in electronic skin," *npj Flex. Electron.*, vol. 3, no. 1, p. 8, Apr. 2019, doi: 10.1038/s41528-019-0051-7.

[44] X. Zhao *et al.*, "A Fully Flexible Intelligent Thermal Touch Panel Based on Intrinsically Plastic Ag 2 S Semiconductor," *Adv. Mater.*, vol. 34, no. 13, Apr. 2022, doi: 10.1002/adma.202107479.

[45] N. Musa *et al.*, "A systematic review and Meta-data analysis on the applications of Deep Learning in Electrocardiogram," *J. Ambient Intell. Humaniz. Comput.*, vol. 14, no. 7, pp. 9677–9750, Jul. 2023, doi: 10.1007/s12652-022-03868-z.

[46] H. Li and P. Boulanger, "A Survey of Heart Anomaly Detection Using Ambulatory Electrocardiogram (ECG)," *Sensors*, vol. 20, no. 5, p. 1461, Mar. 2020, doi: 10.3390/s20051461.

[47] J. Pan and W. J. Tompkins, "A Real-Time QRS Detection Algorithm," *IEEE Trans. Biomed. Eng.*, vol. BME-32, no. 3, pp. 230–236, Mar. 1985, doi: 10.1109/TBME.1985.325532.

[48] D. T. Phan *et al.*, "A Flexible, Wearable, and Wireless Biosensor Patch with Internet of Medical Things Applications," *Biosensors*, vol. 12, no. 3, p. 139, Feb. 2022, doi: 10.3390/bios12030139.

[49] I. Wicaksono *et al.*, "A tailored, electronic textile conformable suit for large-scale spatiotemporal physiological sensing in vivo," *npj Flex. Electron.*, vol. 4, no. 1, p. 5, Apr. 2020, doi: 10.1038/s41528-020-0068-y.

[50] C. Wan *et al.*, "A Flexible and Stretchable 12-Lead Electrocardiogram System with Individually Deformable Interconnects," *Adv. Mater. Technol.*, vol. 7, no. 3, Mar. 2022, doi: 10.1002/admt.202100904.

[51] Z. Huang *et al.*, "Three-dimensional integrated stretchable electronics," *Nat. Electron.*, vol. 1, no. 8, pp. 473–480, Aug. 2018, doi: 10.1038/s41928-018-0116-y.

[52] S. Yao *et al.*, "A Wearable Hydration Sensor with Conformal Nanowire Electrodes," *Adv. Healthc. Mater.*, vol. 6, no. 6, Mar. 2017, doi: 10.1002/adhm.201601159.

This article has been accepted for publication in IEEE Internet of Things Journal. This is the author's version which has not been fully edited and content may change prior to final publication. Citation information: DOI 10.1109/JIOT.2024.3350022

Srinivas Gandla received his M.Sc. degree in Applied Electronics from the Department of Physics at Osmania University, Telangana, India, in 2009. He earned his Ph.D. degree in the Department of Metallurgical Engineering and Materials Science from the Indian Institute of Technology Bombay, India, in 2017. Currently, he is a postdoctoral researcher in the Department of Advanced Materials Science and Engineering at Sungkyunkwan University, Suwon, Korea. His current research areas include physically unclonable functions, thin-film transistors, flexible and stretchable electronic devices, and sensors.

Sunju Kang received her B.Sc. degree in physics from Hannam University in Daejeon, South Korea, in 2014. Since 2018, currently, she is working toward the combined master and Ph.D. degree in Advanced Material Science and Engineering at Sungkyunkwan University, Suwon, South Korea. Her research interests include flexible and stretchable electronic devices and sensors for Human–Machine Interactions.

Junho Kim received his B.S. degree from the School of Electrical and Electronics Engineering at Chung-Ang University, South Korea, in 2018. He is currently a M.S./Ph.D. student in the School of Interdisciplinary Bioscience and Bioengineering at Pohang University of Science and Technology (POSTECH, Pohang, South Korea) under the supervision of Prof. Sung-Min Park. His main research interest is developing medical devices.

Yunjeong Yu received the B.Sc. degree in Material Science and Engineering from Dankook University in Cheonan, South Korea, in 2021. Since 2022, currently she is working toward the master degree in Advanced Material Science and Engineering at Sungkyunkwan University, Suwon, South Korea. Her research interests include flexible and stretchable electronic devices and sensors.

Jaeseong Kim received his B.Sc. degree from the Department of Plant & Environmental New Resources from Kyung-Hee University in Suwon, South Korea, in 2022. Since 2022, currently he is working toward the combined master and Ph.D. degree in Advanced Material Science and Engineering at Sungkyunkwan University, Suwon, South Korea. His research interests include flexible and stretchable electronic devices and sensors for Human-Digital interactive devices, photodetectors and image sensors.

Hyeongtae Lim received his B.Sc. degree in engineering from Daegu Gyeongbuk Institute of Science & Technology (DGIST), South Korea, in 2021. Currently, he is working toward the combined master's and Ph.D. degrees in Electrical Engineering and Computer Science at DGIST. His research interests include flexible platforms, sensors, and next-generation electronic materials.

Hyuk-Jun Kwon received his Ph.D. degree in nanoscale science and engineering from the University of California, Berkeley, in 2015. Earlier, he worked with Samsung Advanced Institute of Technology (SAIT) for two years. Then, he worked for Lam Research (Fremont, CA USA). He has been an associate professor in the Department of Electrical Engineering and Computer Science at DGIST, South Korea, since 2021. His research interests include future semiconductor manufacturing equipment and processes, next-generation electrical devices with flexible/wearable platforms, and laser processing.

Sung-Min Park (Senior Member, IEEE) received the B.S. and Ph.D. degrees in electrical and computer engineering from Purdue University, West Lafayette, IN, USA, in 2001 and 2006, respectively. He has been a Professor with the Department of Convergence IT Engineering and Electrical Engineering, Pohang University of Science and Technology (POSTECH), Pohang, South Korea, since 2016. From 2006 to 2014, he was with Medtronic, Minneapolis, MN, USA, as the Research and Development Manager, leading an Award-Wining Team in developing the world's first MRI conditional pacemaker. From 2014 to 2016, he was with Samsung, Suwon, South Korea, as the Director, spearheading healthcare-centric mobile device and mobile health service platform development projects. His current research interests include developing implantable medical devices, artificial pancreas systems, digital healthcare, and AI-based closed-loop algorithm.

Sunkook Kim received his Ph.D. degree from the Department of Electrical and Computer Engineering of Purdue University in Indiana, USA in 2009. He has been an associate professor at the School of Advanced Materials Science & Engineering of Sungkunkwan University in Suwon, South Korea since 2017. His research interests include augmented human electronics, next-generation high-mobility devices, and nanomaterials. He has authored or co-authored over 200 technical journal articles and conference papers.

This article has been accepted for publication in IEEE Internet of Things Journal. This is the author's version which has not been fully edited and content may change prior to final publication. Citation information: DOI 10.1109/JIOT.2024.3350022

Figures Captions

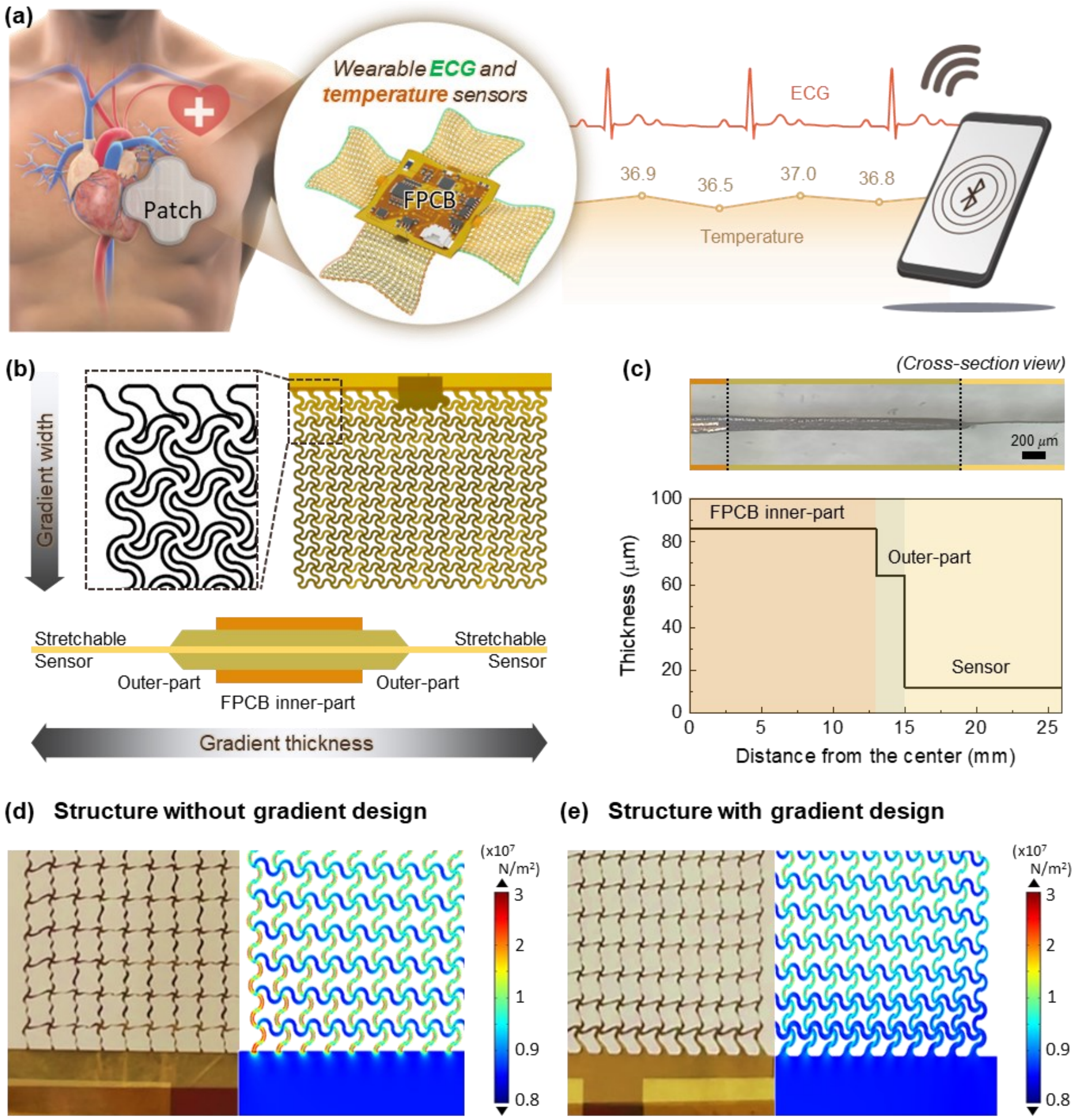

Fig. 1. Overview of the bonding-free robust interface for physiological monitoring. (a) Wearable device for real-time continuous temperature and ECG monitoring. (b) In- and out-of-plane gradient structure designs; the in-plane mesh pattern has gradient serpentine widths. (c) Wearable device with a gradient thickness from the center of the FPCB toward the stretchable sensors (c). (d, e) Real sample and the corresponding FEM simulation of structures without and with gradient designs.

This article has been accepted for publication in IEEE Internet of Things Journal. This is the author's version which has not been fully edited and content may change prior to final publication. Citation information: DOI 10.1109/JIOT.2024.3350022

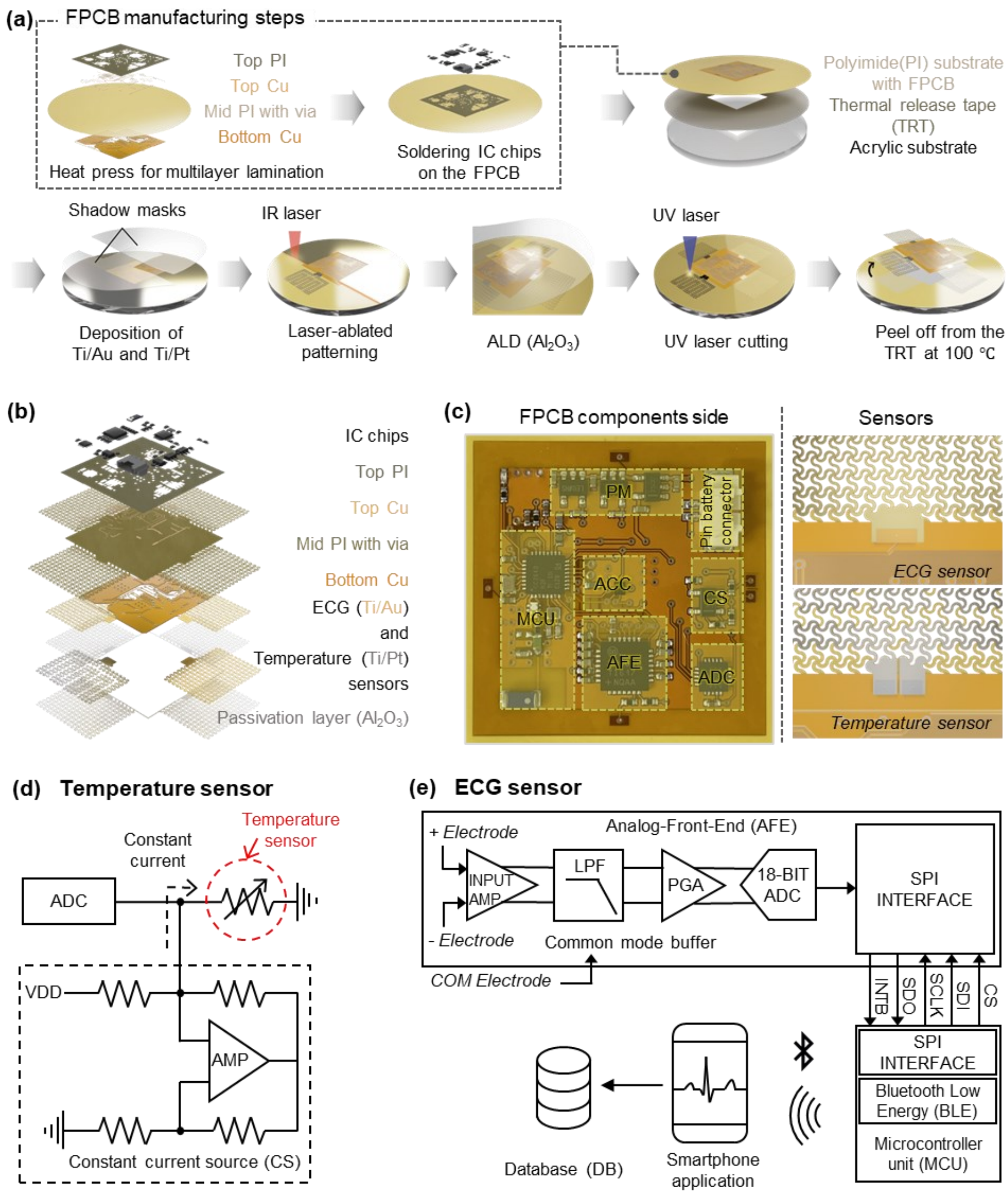

Fig. 2. Fabrication, components, and signal processing of the wearable device. (a) Step-by-step fabrication process, starting from the FPCB manufacture to the fabrication of stretchable temperature and ECG sensors. (b) Schematic layer-by-layer view of the wearable device. (c) FPCB components and bonding-free parts. (d) Signal processing circuit diagram of the temperature and ECG sensors.

This article has been accepted for publication in IEEE Internet of Things Journal. This is the author's version which has not been fully edited and content may change prior to final publication. Citation information: DOI 10.1109/JIOT.2024.3350022

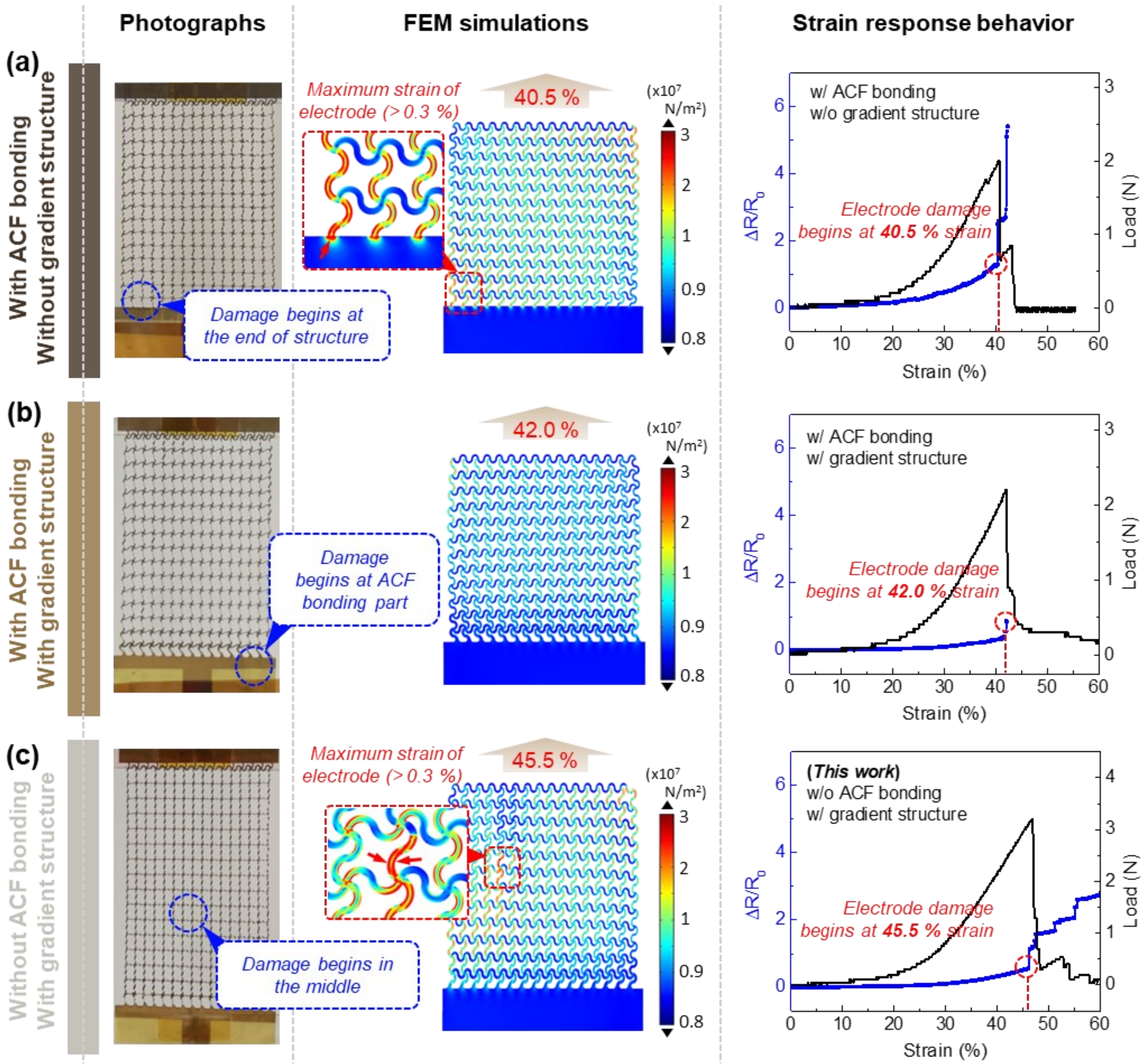

Fig. 3. Mechanics of serpentine-based mesh pattern structures. (a–c) Real images, FEM simulation results, and electrical resistance and load variations to applied strain behavior with (with and without a gradient structure) and without (with a gradient structure) ACF bonding.

This article has been accepted for publication in IEEE Internet of Things Journal. This is the author's version which has not been fully edited and content may change prior to final publication. Citation information: DOI 10.1109/JIOT.2024.3350022

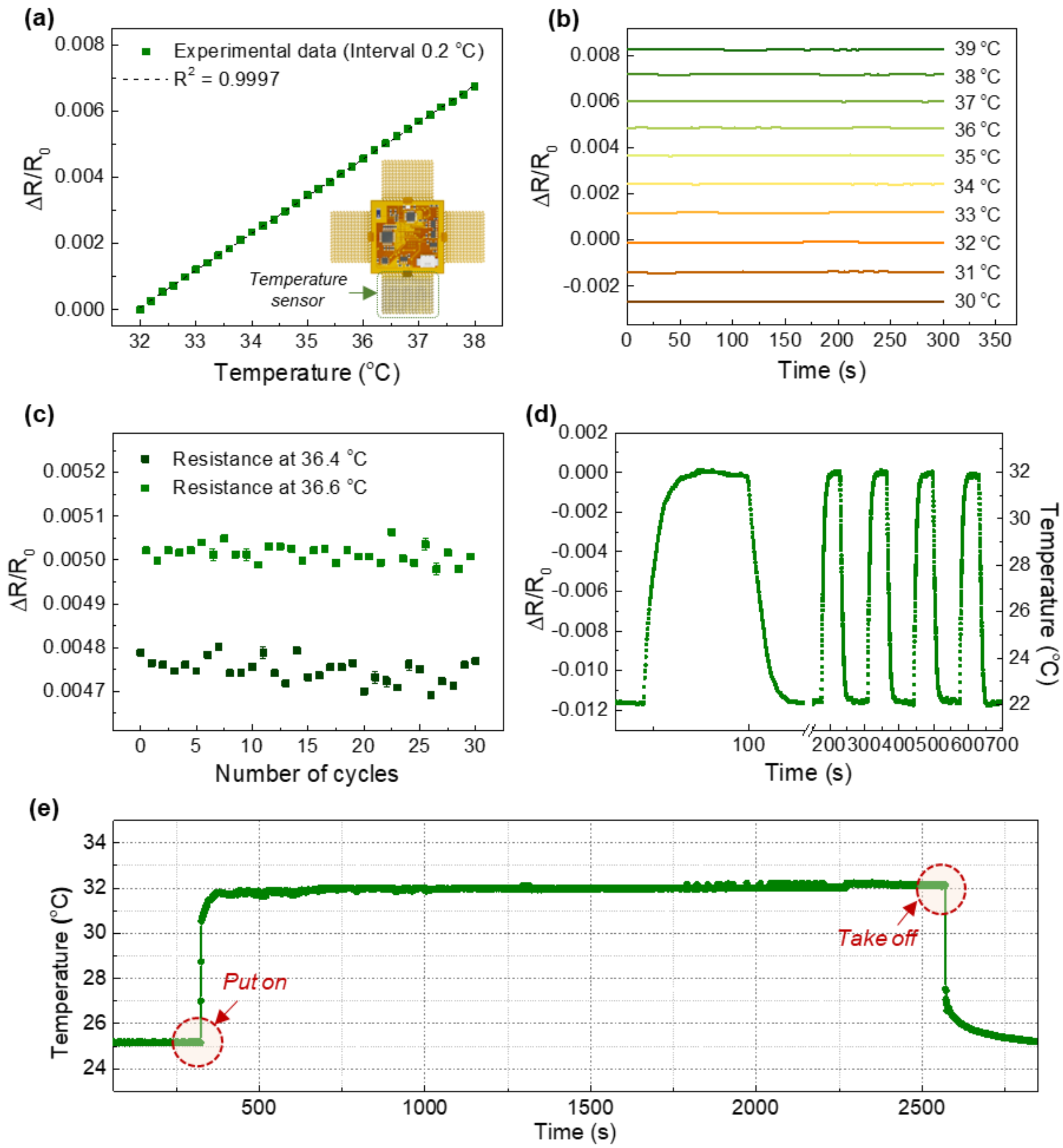

Fig. 4. Electrical characteristics of the temperature sensor. (a) Relative change in resistance to the temperature changes in intervals of 0.2 °C. (b) Stability of the temperature sensor. Sensor response under (c) static and (d) dynamic temperature measurements. (e) Real-time monitoring data of body temperature.

This article has been accepted for publication in IEEE Internet of Things Journal. This is the author's version which has not been fully edited and content may change prior to final publication. Citation information: DOI 10.1109/JIOT.2024.3350022

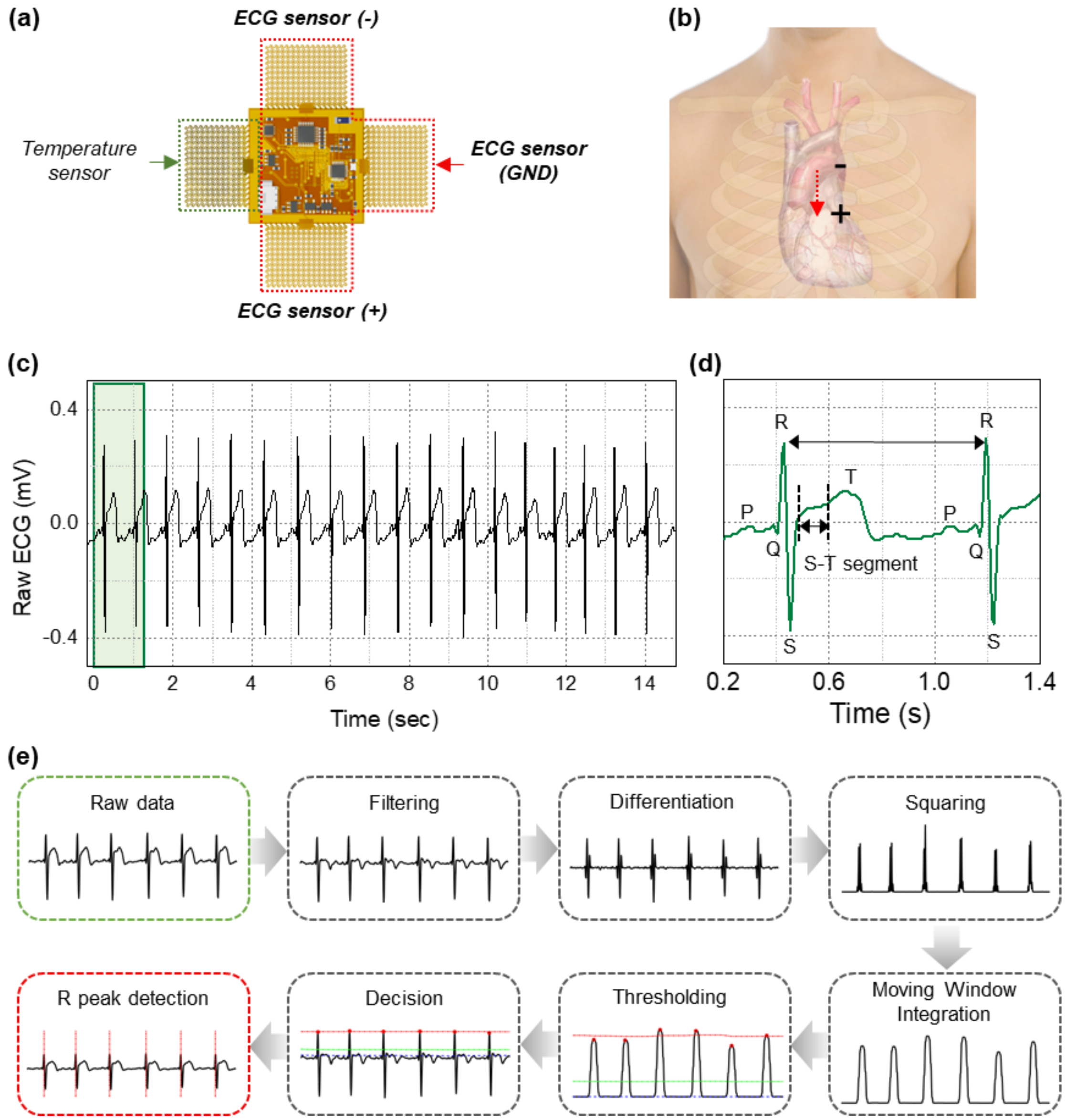

Figure 5. Real-time acquisition of ECG signals through the wearable device. (a) Wearable device showing the temperature (left) and ECG (positive, negative, and ground) sensing electrodes for sensing. (b) Positive and negative signs represent the placement of ECG electrodes for monitoring. (c) Raw ECG data acquired from the wearable device attached to the left side of the chest, as shown in (b). (d) Detailed view of PQRST peak identification and ST-segment. (e) Overview of ECG signal processing.

This article has been accepted for publication in IEEE Internet of Things Journal. This is the author's version which has not been fully edited and content may change prior to final publication. Citation information: DOI 10.1109/JIOT.2024.3350022

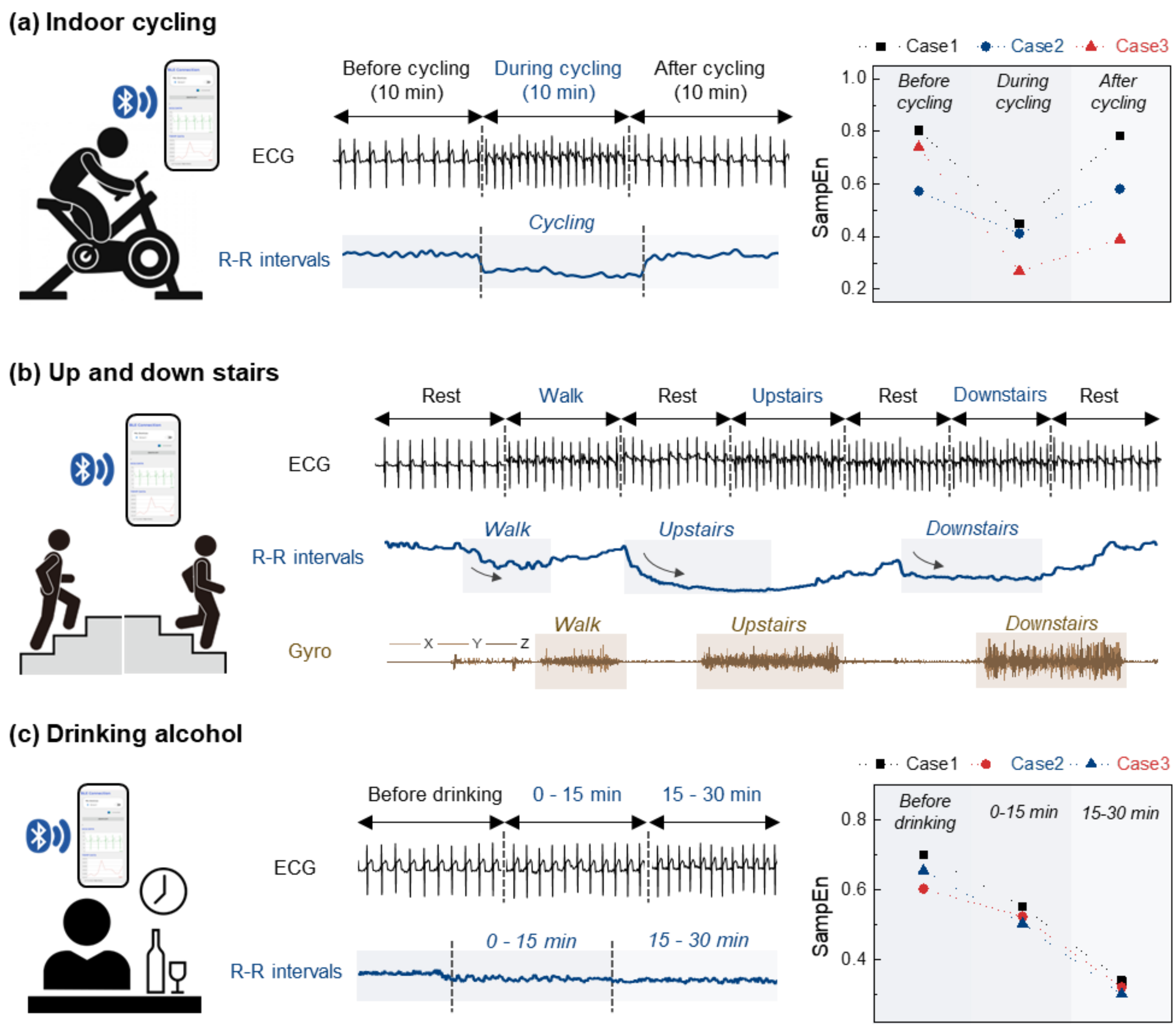

Figure 6. Electrophysiological monitoring during various activities: (a) indoor cycling, (b) walking up and down stairs, and (c) drinking alcohol. Three volunteers (cases 1–3) participated in indoor cycling and drinking alcohol studies.